Time resolved visualization of liquid jet interaction with H_2-air rotating detonations using MHz rate diesel PLIF

Venkat Athmanathan[1a], Matthew Hoeper[2a], Austin Webb[3a], Bebe Wang[4a], Sukesh Roy[5b], H. Douglas Perkins[6c] Christopher A. Fugger[7b] and Terrence R. Meyer[8a]

[a]*Purdue University, West Lafayette, Indiana 47907, USA*

[b]*Spectral Energies, LLC, Beavercreek, Ohio 45430, USA*

[c]*NASA Glenn Research Center, Cleveland, Ohio 44135, USA*

The characterization of the dynamic response of liquid jets to transient detonation wave passage is critical for optimization and modeling of liquid fueled rotating detonation combustors. In this work, a rotating detonation combustor (RDC) is operated on hydrogen and air to sustain stable detonation waves that acts as a detonation driver and interact in a one-way coupled manner with a single liquid fuel jet that propagates into the combustion chamber with cycle periods of ~ 250 µs. Diesel is utilized as a realistic fuel surrogate with higher aromatic compounds to enable fluorescence excitation, using the 355 nm third-harmonic output of a burst-mode Nd:YAG laser, imaged at rates up to 1 MHz. By optimizing the technique to accommodate orders of magnitude variations in the fuel density throughout the injection process, the PLIF data enable quantitative measurements including the refill time, the relative recovery between liquid and gaseous jets and jet trajectory across various momentum flux ratio. As the passage of the detonation wave imparts significant changes in the momentum flux ratio, the qualitative liquid break-up process and spatial distribution varies significantly in time. As the injection system recovers ~ 70% of the cycle period and return to a quasi-steady position and allow comparisons with theoretical jet trajectories. These data, enabled by ultra-high-speed PLIF imaging, represent some of the first detailed measurements for quantifying the dynamic response and recovery of liquid jets exposed to periodic detonations in an operating RDC.

1. Introduction

Rotating detonation combustors, in which a rotating shock is continuously burning the reactants, can theoretically lead to increased gas turbine cycle efficiencies from operating in a valveless constant volume combustion [1–7]. Over the past decade, substantial research has been performed to understand the flow physics within rotating detonation combustors over a wide range of operating conditions for premixed [8,9] as well as non-premixed systems, both numerically and [6,10–14] experimentally[1,2,15–24].

The injectors in non-premixed RDEs are subjected to unsteady impulses from the detonation wave. The pressure in the wake of the detonation wave is typically higher than the injection pressure which causes momentary reactant backflow into the injection system. This causes periodic stoppage of reactant admittance into the combustion chamber.

[1] Research Scientist, School of Mechanical Engineering, Zucrow Labs, Purdue University, AIAA Member.

[2] PhD Student, School of Mechanical Engineering, Zucrow Labs, Purdue University, AIAA Student Member.

[3] PhD Student, School of Mechanical Engineering, Zucrow Labs, Purdue University, AIAA Student Member.

[4] PhD Student, School of Mechanical Engineering, Zucrow Labs, Purdue University, AIAA Student Member.

[5] Senior Research Scientist and CEO, Spectral Energies, LLC, 4065 Executive Dr. Beavercreek, OH 45430, USA, AIAA Associate Fellow

[6] Aerospace Research Engineer, Research and Engineering Directorate, AIAA Senior Member

[7] Research Engineer, Spectral Energies, LLC, 4065 Executive Dr. Beavercreek, OH 45430, USA AIAA Senior Member

[8] Professor, School of Mechanical Engineering, School of Aeronautics and Astronautics (by courtesy), Zucrow Laboratories, AIAA Associate Fellow.

Eventually, the reactant jet recovers, and the fuel/oxidizer mixture is transported downstream of the of the injector into the combustion chamber. These processes have to occur within one cycle period to sustain the detonation wave which is on the order of several hundred microseconds. While gas phase interactions simply have to overcome the detonation overpressure, mix, and combust at the detonation front, liquid phase reactants have additional phase change processes involved in the recovery process. This added phase change complexity and spray break up physics can lead to local reactant phase stratification resulting in mixtures far from the detonability limit. Detonations can also introduce step changes in the momentum of the reactants which can lead to additional shock/detonation induced spray breakup and secondary atomization effects. These dynamic and interlaced processes are coupled with each other, which can make it difficult to study isolated effects of detonation interaction with liquid sprays. Additionally, differences in the liquid refill/mixing process in one detonation period can affect the refill process for the next, which can lead to periodic variations over multiple wave cycles.

In order to elucidate key liquid injection dynamics in the presence of rotating detonation waves, ultra-high-speed planar laser-induced imaging was performed in an RDC that is operated on hydrogen and air to sustain a stable, cyclically propagating detonation wave, where one of the hydrogen fuel sites is replaced with a liquid jet to introduce a diesel spray that can be visualized using burst-mode planar laser-induced fluorescence at repetition rates up to 1 MHz. First, the RDC operation and imaging diagnostics are introduced. This is followed by a phenomenological description of the fuel spray propagation into the combustor channel across a full detonation cycle. Work is currently underway to describe the detailed characteristics of the unsteady fuel spray, including the cessation of fuel injection into the channel, the recovery time in response to the passage of the detonation wave, the dynamic rate of fuel propagation, and the fuel trajectory prior to detonation wave arrival for a range of mass flow rates and injector conditions. Additionally, qualitative features, such as the primary jet breakup process and fuel distribution characteristics will also extensively discussed to understand the impact of the detonation wave passage on the liquid jet varies throughout the cycle.

2. Experimental Setup

(i) Brief description RDC geometry

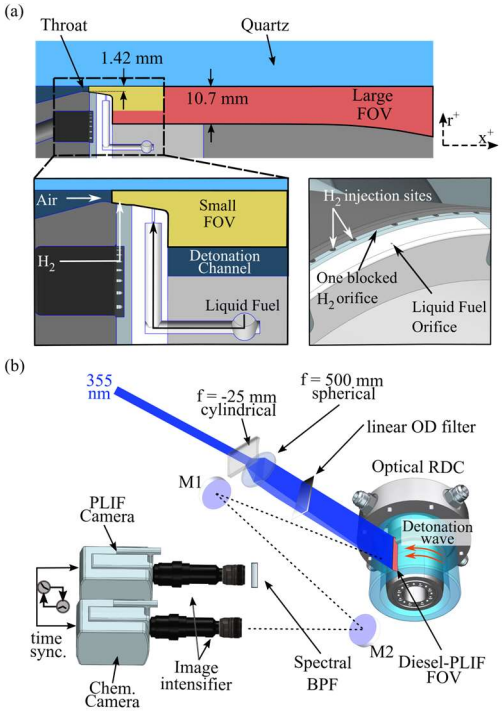

Figure 1: (a) RDC cross-section views showing the detonation channel, with enhanced injector views showing the liquid fuel injector. (b) Laser and optical arrangement for the PLIF and chemiluminescence imaging.

The current RDC geometry and its general operation have been described in previous works [25–27], and a brief description is provided here for reference. A schematic cross-section of the optically accessible RDC is shown in Fig. 1 (a). A ~20 mm thick quartz outer body with an inner diameter of 136 mm serves as the outer wall for the annular detonation channel with a radial passage width of 10.7 mm. Air enters from a plenum through an annular converging-diverging section with a throat gap of 1.42 mm. Immediately downstream of the air throat, gaseous hydrogen fuel is injected radially outward through 100 equally spaced orifices. The injector flow channel at first expands (at 10°) leading into the combustor channel and finally fully expands into the combustor with a backward facing step (BFS). The detonation channel length is ~90 mm (from BFS to combustor exit). Ignition is initiated by an O_2-H_2 pre-detonator originating from the centerbody.

(ii) Liquid injector

A single jet of liquid diesel fuel is injected into the RDC to approximate one-way coupling of the hydrogen-air rotating detonation waves with the fuel jet. One of the hydrogen fuel injection sites is removed and replaced with the orifice for the liquid jet. As shown in Fig.1, this liquid fuel orifice is located at the same azimuth location as the blocked hydrogen orifice and 4.1 mm axially downstream. The internal geometry of the liquid fuel injector is cylindrical, with an orifice exit diameter of 0.3 mm and a length-to-diameter ratio of 10. The liquid fuel orifice is fed by a 2 mm diameter plenum with a length of 13.7 mm. The liquid fuel is supplied to this plenum from internal passages within the RDC centerbody and is metered and controlled close to the RDC. The mass flow rate of liquid fuel is calculated using an experimentally determined discharge coefficient of 0.26 and a pressure measurement upstream of the injector

(iii) Laser System and Optical Arrangement

High-speed imaging of the liquid diesel jet was performed using 355-nm planar laser-induced fluorescence (PLIF) imaging, as shown in Fig. 1 (b). The use of diesel for PLIF has been reported for dynamic imaging of fuels sprays in internal combustion engine environments at rates up to 50 kHz without added tracers [28]. In the current work, a high-power burst-mode Nd: YAG lasers frequency-tripled 355-nm output was used to excite the diesel fuel in the detonation channel. The laser was operated at repetition rates of either 200 kHz or 1 MHz with typical burst lengths of 1500 μs and 750 μs, respectively. The 355 nm output energy at 200 kHz and 1 MHz was ~4.5 mJ/pulse and ~520 μJ/pulse, respectively. A laser sheet was formed using a f=-25 mm cylindrical and f=500 mm spherical lenses, resulting in a ~ 1 mm sheet thickness in the detonation channel. The laser sheet location is centered on the liquid fuel orifice.

Two imaging schemes were implemented to capture small-scale and large-scale spray characteristics. The first scheme at a 200 kHz repetition rate had a field of view (FOV) that covered approximately the entire axial (x) length of the detonation channel. For this, the diesel PLIF used a high-speed Phantom v2012 camera paired with a high-speed image intensifier (Lambert, HiCatt), a 85 mm f/1.8 visible camera lens, a 420 nm longpass optical filter, and used a 40 ns exposure. For the broadband chemiluminescence imaging, a second high-speed Phantom v2012 camera was paired with a high-speed UV intensifier (LaVision IRO), a 105 mm UV f/4.5 camera lens, and used a 100 ns exposure.

The second imaging scheme was at a 1 MHz repetition rate and the diesel PLIF had a much smaller FOV around the liquid injection site. For this scheme, an ultra-high-speed Shimadzu HPV-X2 camera was used with a 200 mm f/4 lens, a 420 nm longpass optical filter, and a 100 ns camera exposure. Due to the relatively dense spray in this region, the PLIF signal was sufficient to not need the use of an image intensifier. The 1 MHz broadband chemiluminescence imaging utilized a second Shimadzu HPV-X2 camera, a high-speed UV intensifier (LaVision IRO), a 105 mm UV f/4.5 camera lens, and a 100 ns exposure.

The PLIF measurements are made on the radial-axial (r-x) plane of the detonation channel. The chemiluminescence view is of a tangential plane (θ-x) that is centered on and perpendicular to the PLIF plane. For the 200 kHz imaging, the laser sheet intensity profile was tailored in the x direction using a continuously variable neutral density filter such that the laser energy was lowest in the near field and highest in the far field, as shown in Fig. 1. This approach minimized camera saturation from the near-field dense spray while allowing sufficient signal in the lower-density far-field region.

(iv) Test matrix description

The operating conditions for comparing the two injection systems is shown in Table 1. The total flow rate through the combustor was maintained at 0.44 kg/s and 0.22 kg/s at stoichiometric fuel/air conditions. The injection pressure was systematically varied to understand the effect of 'steady-state' momentum flux ratio on the injection refill process.

Table 1: Operating conditions for the study

Test #	Configuration.	$G_{air\text{-}throat}$ (kg/m^2/s)	$\dot{m}_{air}$ (kg/s)	ϕ_{global}	Liquid flow rate (g/s)	Liquid inj. P (bar)	q
1	BFS – 90° injection	785	0.46	1.04	0.92	16	0.057
2		785	0.46	0.99	0.67	9.2	0.030
3		785	0.45	1.06	0.43	4.3	0.012
4		370	0.23	1.03	0.67	8.5	0.058

3. Current work:

(v) Phenomenological Description:

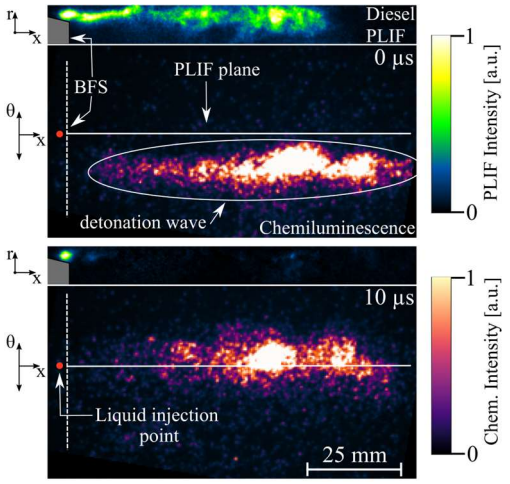

Figure 2: Fuel spray and chemiluminescence images immediately before and after the wave passage.

A phenomenological description of the liquid fuel jet and its evolution in time is provided to highlight the unsteady fuel spray behavior in response to the passage of the detonation wave. The simultaneous diesel-PLIF and chemiluminescence images in Fig. 2 show that the spray has filled ~60% of the detonation channel just prior to the arrival of the detonation wave. Note that while the fluorescence intensity is relatively uniform along the axial direction, based on the nonlinear scaling in, the diesel fluorescence intensity in the axial far-field region is about two-orders of magnitude weaker than in the near-field of the injector due to spray break up, dispersion, evaporation, and potentially reactions upon mixing with hot combustion products. Within ~10 µs after the arrival of the detonation wave, the diesel signal is nearly completely extinguished throughout the length of the channel, except in the region closest to the injector orifice. Figure 3 shows a complete cycle with the arrival of the detonation wave near the beginning and end of the sequence, encompassing 250-260 µs. For $x < 30$ mm, the spray is confined toward the outer radius of the channel, and for $x > 30$ mm, the spray expands rapidly to fill much of the channel radial width. This spatial distribution closely follows the mixture evolution of a gas-gas supersonic jet entering the same channel geometry under the same flow conditions [19], indicating that the spray is entrained into and convected downstream by the supersonic air cross flow.

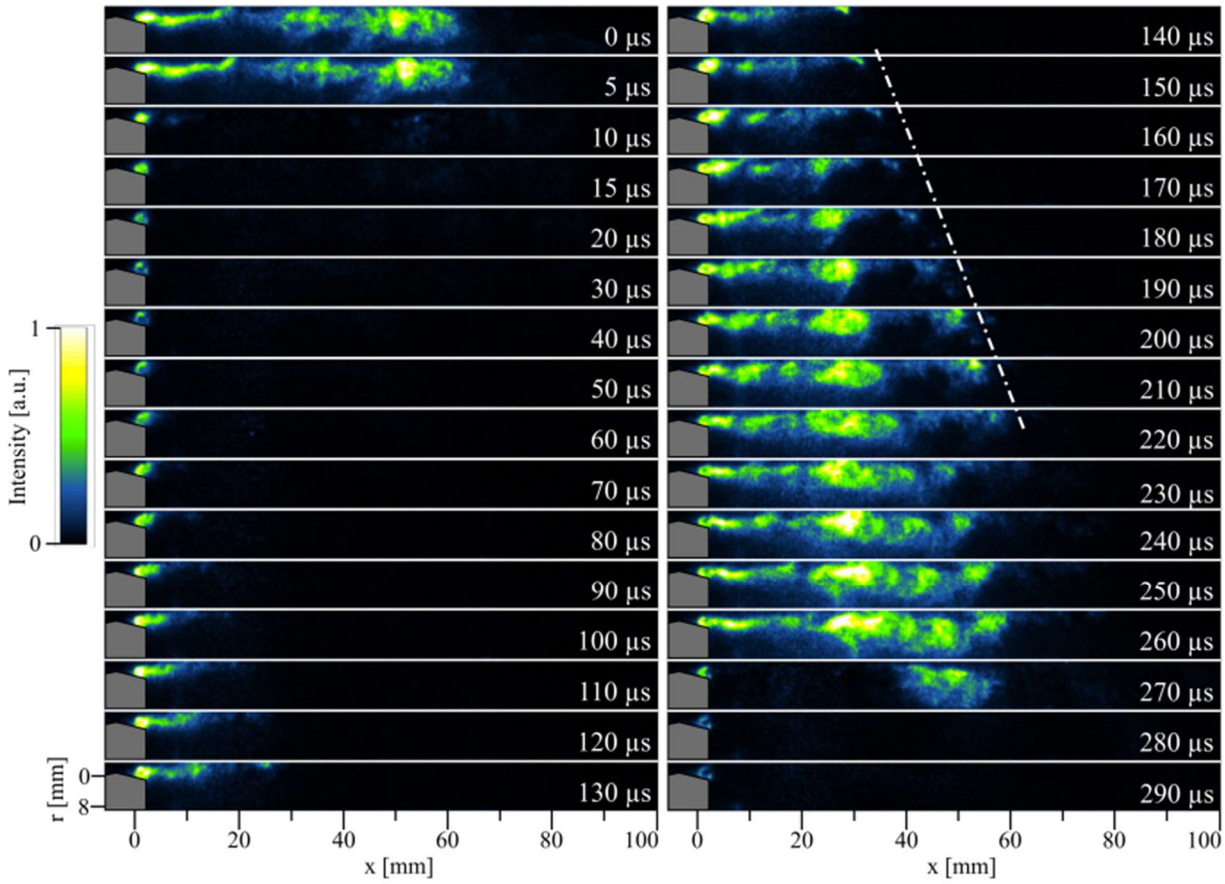

Figure 3: Image sequence of diesel PLIF (Large FOV, 200 kHz) for Case 2 across one detonation cycle period. The frame spacing is ~ 5µs apart.

4. Near-Field Liquid Fuel Jet Trajectory

It is of interest to measure the fuel spray trajectory emmanating from the liquid orifice as this affects the penetration into the air crossflow and subsequent mixing and dispersion across the detonation channel. Moreover, jets in crossflow in unsteady flowfields have been shown to deviate significantly from steady state cases [29]. The fuel spray trajectory is determined from the current data by following the leading edge 25% intensity profile. First, an average is taken of the 40 images prior to the arrival of the detonation wave as it was observed that the spray is mostly fully recovered by this time (its trajectory and spray characteristics did not vary significantly with time). The leading edge spray profile (i.e., the fuel spray penetration) was then tabulated for the different test cases. For reference, penetration heights are compared with an experimentally derived correlation for a spray jet in crossflow in a bluff configuration [30], as shown in Equation 1.

$$y/d = (1.2+0.4d)q0.36\ \ln[1+(1.56+0.48d)(x/d)]$$

where q is the momentum flux ratio between the air and the liquid diesel, d is the liquid orifice diameter, and x and y are the axial and radial trajectory coordinates, respectively. As shown in Fig. 4, as the time-averaged liquid jet to air crossflow momentum flux ratio increases, the near field fuel spray penetration height increases, as expected. While this trend appears to be reasonably well predicted by the empirical correlation, there are significant deviations from a canonical jet-in-crossflow trajectory. Noticeably, there is a significant change in jet penetration after the backward facing step. As q and the penetration height decreases, the fuel spray is entrained into the shear layer formed

between the incoming reactants and the wake formed behind the backward facing step. Moreover, this trajectory is valid prior to the detonation wave arrival, but during and shortly after the passage of the detonation wave, the jet trajectory is not well predicted by the correlation (not shown).

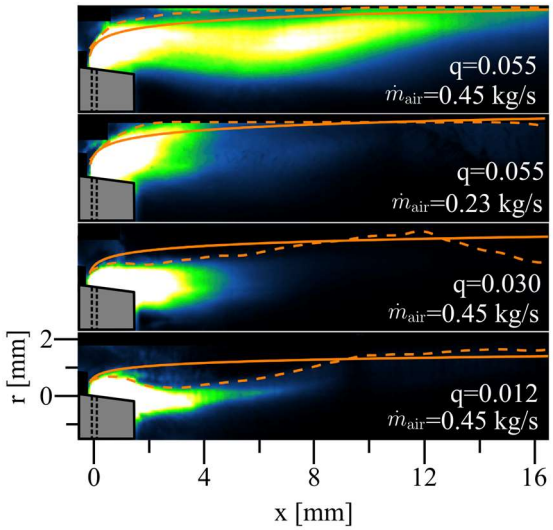

Figure 4: Experimental penetration (dashed line) compared to empirical correlation (solid line) for various momentum flux ratios overlaid on time averaged images for two air mass flow rate cases (0.23 kg/s and 0.45 kg/s) and three liquid jet to air crossflow momentum flux ratio cases (q = 0.012, 0.030, and 0.055).

5. Future analysis:

While data collection has been completed in the last few months, data analysis is currently being undertaken and will be included in the final form of the manuscript. The following specifics will be added to the main document:

- Comparison of liquid jet recovery at various mass flow rates and injection pressure ratios
- Database of refill and recovery times for various mass flow rates and injection pressure.
- Further discussion and comparison of current dataset to correlations for liquid jet in supersonic cross flow environment.
- Analysis on detonation wave strength after passing the liquid jet using high-frequency pressure transducer measurements.

We expect the aforementioned analysis to be completed in the next few months for a comprehensive and complete description of the liquid jet – detonation interaction phenomena.

6. Acknowledgement

This work was funded by NASA under STTR contract 80NSSC21C0031.The authors would like to acknowledge experimental assistance from Zach Ayers, Purdue University. Funding for equipment was provided, in part, under AFOSR Award No. FA9550-16-1-0315 (Dr. Martin Schmidt, Program Officer).

7. References

[1] Anand V, St. George A, Driscoll R, Gutmark E. Investigation of rotating detonation combustor operation with H2-Air mixtures. Int J Hydrogen Energy 2016;41:1281–92. https://doi.org/10.1016/j.ijhydene.2015.11.041.

[2] Bach E, Stathopoulos P, Paschereit CO, Bohon MD. Performance analysis of a rotating detonation combustor based on stagnation pressure measurements. Combust Flame 2020;217:21–36. https://doi.org/10.1016/j.combustflame.2020.03.017.

[3] Sato T, Chacon F, White L, Raman V, Gamba M. Mixing and detonation structure in a rotating detonation engine with an axial air inlet. Proc Combust Inst 2020. https://doi.org/10.1016/j.proci.2020.06.283.
[4] Bykovskii FA, Zhdan SA, Vedernikov EF. Continuous spin detonations. J Propuls Power 2006;22:1204–16. https://doi.org/10.2514/1.17656.
[5] Peng HY, Liu WD, Liu SJ, Zhang HL, Zhou WY. Realization of methane-air continuous rotating detonation wave. Acta Astronaut 2019;164:1–8. https://doi.org/10.1016/j.actaastro.2019.07.001.
[6] Shao YT, Liu M, Wang JP. Numerical investigation of rotating detonation engine propulsive performance. Combust Sci Technol 2010;182:1586–97. https://doi.org/10.1080/00102202.2010.497316.
[7] Kailasanath K. Recent Developments in the Research on Pressure-Gain Combustion Devices. In: Gupta AK, De A, Aggarwal SK, Kushari A, Runchal A, editors. Innov. Sustain. Energy Clean. Environ., Singapore: Springer Singapore; 2020, p. 3–21. https://doi.org/10.1007/978-981-13-9012-8_1.
[8] Andrus IQ. A Premixed Rotating Detonation Engine: Design and Experiment n.d.
[9] Liu Z, Braun J, Paniagua G. Characterization of a Supersonic Turbine Downstream of a Rotating Detonation Combustor. J Eng Gas Turbines Power 2018;141:031501. https://doi.org/10.1115/1.4040815.
[10] Braun J, Saracoglu BH, Paniagua G. Unsteady Performance of Rotating Detonation Engines with Different Exhaust Nozzles. J Propuls Power 2017;33:121–30. https://doi.org/10.2514/1.B36164.
[11] Nordeen CA, Schwer D, Schauer F, Hoke J, Barber T, Cetegen B. Thermodynamic model of a rotating detonation engine. Combust Explos Shock Waves 2014;50:568–77. https://doi.org/10.1134/S0010508214050128.
[12] Lietz CF, Desai Y, Hargus W, Sankaran V. Parametric investigation of rotating detonation rocket engines using large eddy simulations. AIAA Propuls. Energy Forum Expo. 2019, American Institute of Aeronautics and Astronautics Inc, AIAA; 2019. https://doi.org/10.2514/6.2019-4129.
[13] Batista A, Ross MC, Lietz C, Hargus WA. Descending Modal Transition Dynamics in a Large Eddy Simulation of a Rotating Detonation Rocket Engine. Energies 2021, Vol 14, Page 3387 2021;14:3387. https://doi.org/10.3390/EN14123387.
[14] Sato T, Voelkel S, Raman V. Detailed Chemical Kinetics Based Simulation of Detonation-Containing Flows, ASME International; 2018. https://doi.org/10.1115/gt2018-75878.
[15] Athmanathan V, Rahman KA, Lauriola DK, Braun J, Paniagua G, Slipchenko MN, et al. Femtosecond/picosecond rotational coherent anti-Stokes Raman scattering thermometry in the exhaust of a rotating detonation combustor. Combust Flame 2021;231:111504. https://doi.org/10.1016/j.combustflame.2021.111504.
[16] Tobias J, Depperschmidt D, Welch C, Miller R, Uddi M, Agrawal AK, et al. OH* Chemiluminescence Imaging of the Combustion Products From a Methane-Fueled Rotating Detonation Engine 2019. https://doi.org/10.1115/1.4041143.
[17] Bohon MD, Bluemner R, Paschereit CO, Gutmark EJ. Measuring Rotating Detonation Combustion Using Cross-Correlation. Flow, Turbul Combust 2019;103:271–92. https://doi.org/10.1007/s10494-019-00017-z.
[18] Peng WY, Cassady SJ, Strand CL, Goldenstein CS, Spearrin RM, Brophy CM, et al. Single-ended mid-infrared laser-absorption sensor for time-resolved measurements of water concentration and temperature within the annulus of a rotating detonation engine. Proc Combust Inst 2019;37:1435–43. https://doi.org/10.1016/j.proci.2018.05.021.
[19] Mathews GC, Blaisdell MG, Lemcherfi AI, Slabaugh CD, Goldenstein CS. High-bandwidth laser-absorption measurements of temperature, pressure, co, and h2o in the annulus of a rotating detonation rocket engine. AIAA Scitech 2021 Forum 2021:1–11. https://doi.org/10.2514/6.2021-0418.
[20] Ayers ZM, Lemcherfi AI, Plaehn EW, Slabaugh CD, Meyer TR, Fugger CA, et al. Application of 100 khz acetone-plif for the investigation of mixing dynamics in a self-excited linear detonation channel. AIAA Scitech 2021 Forum, American Institute of Aeronautics and Astronautics Inc, AIAA; 2021, p. 1–11. https://doi.org/10.2514/6.2021-0554.
[21] Nair AP, Lee DD, Pineda DI, Kriesel J, Hargus WA, Bennewitz JW, et al. MHz laser absorption spectroscopy via diplexed RF modulation for pressure, temperature, and species in rotating detonation rocket flows. Appl Phys B Lasers Opt 2020;126:138. https://doi.org/10.1007/s00340-020-07483-8.
[22] Sosa J, Burke R, Ahmed KA, Micka DJ, Bennewitz JW, Danczyk SA, et al. Experimental evidence of H2/O2 propellants powered rotating detonation waves. Combust Flame 2020;214:136–8. https://doi.org/10.1016/j.combustflame.2019.12.031.
[23] Chacon F, Gamba M. Development of an optically accessible continuous wave rotating detonation engine. 2018 Jt. Propuls. Conf., [publishername] American Institute of Aeronautics and Astronautics Inc, AIAA; 2018. https://doi.org/10.2514/6.2018-4779.

[24] Schwinn K, Gejji R, Kan B, Sardeshmukh S, Heister S, Slabaugh CD. Self-sustained, high-frequency detonation wave generation in a semi-bounded channel. Combust Flame 2018;193:384–96. https://doi.org/10.1016/j.combustflame.2018.03.022.
[25] Sousa J, Braun J, Paniagua G. Development of a fast evaluation tool for rotating detonation combustors. Appl Math Model 2017;52:42–52.
[26] Wang RZJ. Numerical investigation of shock wave reflections near the head ends of rotating detonation engines 2013:461–72. https://doi.org/10.1007/s00193-013-0440-0.
[27] Katta VR, Cho KY, Hoke JL, Codoni JR, Schauer FR, Roquemore WM. Effect of increasing channel width on the structure of rotating detonation wave. Proc Combust Inst 2019;37:3575–83. https://doi.org/10.1016/j.proci.2018.05.072.
[28] Meyer TR, Brear M, Jin SH, Gord JR. Formation and Diagnostics of Sprays in Combustion. Handb Combust 2010:291–322. https://doi.org/10.1002/9783527628148.HOC031.
[29] A. R. Karagozian, Transverse jets and their control, Prog. Energy Combust. Sci. 36 (5) (2010) 531–553.
[30] C.-W. Lee, S. Moon, C.-H. Sohn, H.-J. Youn, Spray and combustion characteristics of a dump-type ramjet combustor, KSME Inter. J. 17 (12) (2003) 2019–2026.